Tunnelling and Underground Space Technology 95 (2020) 103170

Contents lists available at ScienceDirect

Tunnelling and Underground Space Technology

journal homepage: www.elsevier.com/locate/tust

Yield-power-law fluid propagation in water-saturated fracture networks with application to rock grouting

Liangchao Zou[a,*], Ulf Håkansson[b,c], Vladimir Cvetkovic[a]

[a] Division of Resources, Energy and Infrastructure, Department of Sustainable Development, Environmental Science and Engineering, Royal Institute of Technology, 10044 Stockholm, Sweden
[b] Division of Soil and Rock Mechanics, Department of Civil and Architectural Engineering, Royal Institute of Technology, 10044 Stockholm, Sweden
[c] Skanska AB, 11274 Stockholm, Sweden

ARTICLE INFO

Keywords:
Rock grouting
Two-phase flow
Yield-power-law fluids
Propagation volume fraction
Fracture networks

ABSTRACT

Cement grouting is widely applied in rock tunneling and underground construction to reduce groundwater inflow and increase the tightness of rock masses. The rock grouting process involves complex non-Newtonian grouts propagation in fracture networks. In this study, a two-phase flow model extended for yield-power-law fluid (e.g., cement grout) propagation in water-saturated fracture networks is presented. The effective transmissivity is scaled from analytical solutions for single-phase yield-power-law fluids flow between a pair of smooth parallel plates. This extended two-phase flow model for fracture networks is verified based on a unique set of experimental data. The full experiment dataset is presented in this work for the first time. Impacts of rheological parameters and time-dependent rheological properties of injected yield-power-law fluids on propagation processes are investigated through numerical simulations. A measure referred to as the propagation volume fraction is defined as an indicator of the propagation process. The results generally show that the rheological properties significantly affect the evolution of the propagation volume fraction. The propagation rate reduces with increased yield stress, consistency index and flow index. The two-phase flow of yield-power-law fluid propagation in a heterogeneous fracture network is also simulated, showing that the heterogeneity of fracture apertures may significantly affect the propagation process. For the heterogeneous case, with two-point distribution of apertures, the propagation volume fraction can be represented by using the harmonic mean aperture. Since the yield-power-law constitutive model covers a wide range of non-Newtonian fluids, the results presented in this work can be used for studying non-Newtonian fluid propagation in a variety of homogeneous or heterogeneous fracture networks, which can be used for rock grouting design.

1. Introduction

Non-Newtonian fluid flow through randomized fractures is of interest in a variety of underground engineering practices, such as modeling of rock grouting in underground engineering projects (e.g., Wallner, 1976; Lombardi, 1985; Hässler, 1991; Eriksson et al., 2000; El Tani, 2012; Gustafson et al., 2013; Stille, 2015; Mohajerani et al., 2017; Zhang et al., 2017; Funehag and Thörn, 2018; Xu et al., 2019), and predicting drilling muds spreading in oil and gas extraction (e.g., Frigaard et al., 2017). Particularly, cement grouting for subsurface formations is an increasingly interesting application field due to stringent demands for controlling groundwater flow in underground structures or constructions. (Gustafson et al 2013; Sui et al., 2015; Stille 2015; Li et al., 2016; Xu et al., 2019; Bohloli et al., 2019). In many cases dams of all sizes rest on rock formations. As part of the construction as well as critical maintenance in the case of ageing dams, the underlying geological formations typically require injection of large amounts of cement grouts for flow reduction and stability improvement (e.g., Warner 2004; U.S. Army Corps of Engineers, 2014). Likewise, transportation infrastructure in many urban regions is expanding into underground space, which also requires cement grout injection to avoid adverse effects and to secure optimal functionality (e.g., Hässler et al., 1992; Håkansson et al., 1992; Stille 2015; Li et al., 2016). Finally, construction related to geological disposal most notably of nuclear waste, requires minimizing water flow toward deposition tunnels and canisters once again by injecting large amounts of cement grouts (e.g. Emmelin et al., 2007). In all cases, cement grout injection into a geological formation combines design variables (e.g., type and amount of

* Corresponding author at: Division of Resources, Energy and Infrastructure, Department of Sustainable Development, Environmental Science and Engineering, Royal Institute of Technology, 10044 Stockholm, Sweden.
E-mail address: lzo@kth.se (L. Zou).

https://doi.org/10.1016/j.tust.2019.103170
Received 2 July 2019; Received in revised form 21 October 2019; Accepted 22 October 2019
Available online 02 November 2019
0886-7798/

cement grout, the injection pressure) with complex heterogeneity of the subsurface, notably rock fractures that are typically saturated with water consisting of channelized structures (Hässler et al., 1992; Håkansson et al., 1992; Fidelibus and Lenti 2012; Sui et al., 2015; Zou et al., 2018, 2019).

Fundamental aspects of Newtonian fluid (e.g., groundwater) flow in channelized structures pertinent to geological formations have been studied in both two dimensions (Cacas et al., 1990; Baghbanan and Jing 2007; Dershowitz et al., 2007) and three dimensions (Cvetkovic and Frampton 2012; Dreuzy et al., 2012; Dessirier et al., 2018). However, cement grouts commonly used in engineering practice are often non-Newtonian fluids (Hässler 1991; Håkansson et al., 1992; Nguyen et al., 2006; Balhoff et al., 2012; Rahman et al., 2015; Shamu and Håkansson 2019). The flow of cement grouts occurs only when the shear stress exceeds the yield stress. Most non-Newtonian fluids also exhibit non-linear rheological behavior, such as shear-shinning and shear-thickening, which are commonly approximated by the yield-power-law model, also referred to as the Herschel-Bulkley model (e.g., Herschel and Bulkley, 1926). For completeness, a detailed description of the yield-power-law rheological model is presented in Appendix A. The yield-power-law model contains three parameters, the yield stress, the consistency index k and the flow index n. Particular parameter choices reduce the yield-power-law model to Bingham, power-law or Newtonian models, respectively. The Herschel-Bulkley model is therefore able to represent a wide range of rheological behaviors of non-Newtonian fluids (e.g., Herschel and Bulkley, 1926; Mitsoulis, 2007) that are relevant for different types of grout (e.g., Nguyen et al., 2006; Funehag and Fransson, 2006; Butrón et al., 2009; Rahman et al., 2015; Pedrotti et al., 2017; Liang et al., 2019).

Analytical solutions for single-phase yield-stress or power-law fluid flow in a 1D single channel are available in the literature (e.g., Bird et al., 1960; Huilgol 2015; Panaseti et al., 2018). However, flow of non-Newtonian fluids in geological formations often involves two-phase flow (Hässler et al., 1992; Fidelibus and Lenti 2012; Sui et al., 2015; Zou et al., 2018), and cement grouts are typical examples of yield-power-law fluids (Håkansson, 1993; Nguyen et al., 2006; Rahman et al., 2015; Shamu and Håkansson 2019). Due to the complexity in resolving the two-phase flow problem that involves non-Newtonian fluids penetrating through water-saturated fractures, most of previous studies assumed that the flow of water phase is negligible (e.g., El Tani, 2012; Gustafson et al., 2013; Mohajerani et al., 2017; Xiao et al., 2017). Recently Zou et al., (2018) presented simulations of two-phase flow for Bingham fluid propagation in a single water-saturated fracture, and studied the impact of water phase flow. It was found that the water flow may significantly affect the propagation processes depending on the viscosity ratio between the Bingham fluid and water.

Moreover, most of previous studies only considered the Newtonian grouts (e.g., Funehag and Fransson, 2006) or the Bingham grouts (e.g., Hässler et al., 1992; Eriksson et al., 2000; Gustafson et al., 2013; Fidelibus and Lenti, 2012; Mohajerani et al., 2017). Experimental studies suggest that cement grouts commonly used in practice with the water/cement (w/c) ratio between 0.6 and 0.8 are actually yield-power-law fluids (Håkansson, 1993; Nguyen et al., 2006; Rahman et al., 2015; Shamu and Håkansson, 2019). Some special grouts, such as fine cement grouts with high w/c ratio, i.e., w/c ≥ 1, polymer-modified cement grouts and silica sol, are Newtonian or power-law fluids (Funehag and Fransson, 2006; Li et al., 2016). To date, only a few studies have simulated non-Newtonian grout propagation in fracture networks, e.g., Mohajerani et al. (2017) modeled Bingham grout propagation in 2D discrete fracture networks without consideration of the groundwater flow. By considering groundwater flow, Hässler (1991), and Eriksson et al. (2000) simulated Bingham grout flow in 2D structured fracture networks using an implicit numerical model; Fidelibus and Lenti (2012) developed a numerical pipe network model and modeled Bingham grout propagation in 2D structured networks; Deng et al. (2018) simulated Bingham grout penetration in 3D fracture networks using a computational fluid dynamics (CFD) approach; Zou et al. (2019) simulated Bingham grout propagation in 2D random fracture networks. In general, these studies only considered Bingham grout. Most previous studies have not been validated, except that Hässler (1991), Eriksson et al. (2000), and Mohajerani et al., (2017) compared their simulation results with the experimental data by Håkansson (1987). Therefore, the remaining fundamental questions are related first to the scaling of effects through a system of randomized water-saturated fractures representing pores or fractures in a geological media, and second to the generalizing for the yield-power-law fluids, which represent the broad class of material constitutive law relevant for cement grouts.

In this work, we investigate two-phase flow of yield-power-law fluids through water-saturated randomized fracture networks with application to rock grouting. Our first objective is to generalize the two-phase flow model for a Bingham fluid in a single fracture presented in Zou et al., (2018) to yield-power-law fluids in a network of fractures. Experimental data of cement grout propagation in water-saturated fracture networks conducted on large laboratory scale relevant for applications are rare in the literature. The second objective of this study is to verify the two-phase fracture network model using our own original experiments (Håkansson 1987), presenting for the first time the complete data set of the experiments. Finally, our third and main objective is to investigate the physics of the propagation process, specifically how rheological properties affects yield-power-law fluid propagation through regular as well as randomized fracture networks.

2. Two-phase flow from a single fracture to a fracture network

We consider non-Newtonian fluid flow through a regular fracture network that represents a relatively large-scale geological media. The network consists of single fractures each defined by two smooth parallel plates (Fig. 1). Note that the assumption of smooth parallel plates for rock fractures and regular fracture networks is adopted analogy to previous analytical studies (e.g., Hässler et al., 1992; Eriksson et al., 2000 Fidelibus and Lenti, 2012; El Tani, 2012; Gustafson et al, 2013; Stille, 2015) and the experiment configuration (Håkansson, 1987). The limitation of this assumption is further discussed in Section 6. The two-phase flow model presented by Zou et al. (2018) is briefly introduced as the basis to be extended to fracture networks in this work. Water is

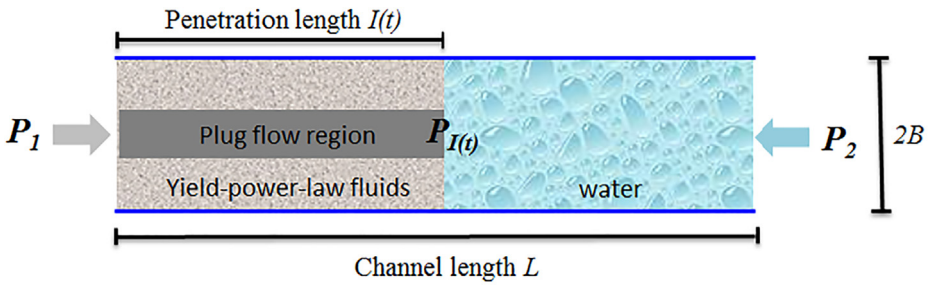

Fig. 1. Schematic illustration of the propagation of a yield-power-law fluid in a single water-saturated fracture, modified from Zou et al. (2018).

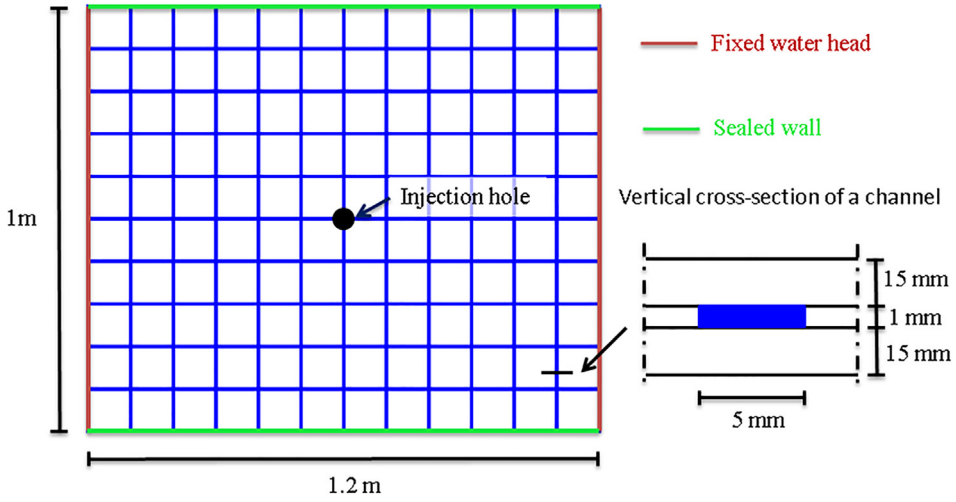

Fig. 2. Schematic illustration of the laboratory test system.

initially present in the fracture and is displaced by a yield-power-law fluid as a moving interface. The pressure difference between the inlet and outlet of a fracture is$P_1 - P_2$. The length of the fracture is L and the aperture is $2B$. The interface represents the location of the propagation front $I(t)$, which describes the water displacement process.

Our basic assumption for this system is that the flow in each fracture is advection- dominated, whereby macro-dispersion is controlled by the heterogeneity of hydraulic properties (fracture apertures). This assumption implies that the propagation process of the injected yield-power-law fluid in a water-saturated fracture is an immiscible two-phase flow and that capillary pressure effects are negligible. Furthermore, we also assume that the injected yield-power-law fluid and groundwater are both incompressible, that gravitational forces and inertial effects are negligible (the flow is laminar) and that the fracture aperture is much smaller than the lateral dimensions (i.e., the pressure gradient across the aperture is negligible by adopting the lubrication approximation). The above assumptions are consistent with how water flow and solute transport are modeled in heterogeneous porous media (Cacas et al., 1990; Baghbanan and Jing 2007; Dershowitz et al., 2007; Dreuzy et al., 2012).

The two-phase flow process in a fracture can be expressed as (Zou et al., 2018)

$$\frac{\partial}{\partial \mathrm{x}} T(C) \frac{\partial P}{\partial \mathrm{x}} = 0 \tag{1}$$

$$u = \frac{T(C)}{2BW} \frac{\partial \mathrm{P}}{\partial \mathrm{x}} \tag{2}$$

$$\frac{\partial C}{\partial t} + u \frac{\partial C}{\partial \mathrm{x}} = 0 \tag{3}$$

where C is a phase function (i.e., $C = 1$ represents the grout phase and $C = 0$ denotes the groundwater phase), t is time, P is pressure, u is velocity, B is half of the fracture aperture, W is the fracture width, and $T$is the effective transmissivity, which has different expressions for different fluid phases, i.e., grout and groundwater. Note that the phase function C used in Eqs. (1) and (2) is to keep the simplicity of the expression for the two-phase flow, which means that the effective transmissivity T is different for different fluids, i.e., grout and groundwater.

For the fracture defined by a pair of parallel plates (Fig. 1), the effective transmissivity T can be determined by analytical solutions of the flowrate for single-phase yield-power-law fluids between smooth parallel plates, using

$$T = \frac{Q}{P_x} \tag{4}$$

where Q is the flowrate and $P_x = \frac{\partial P}{\partial x}$ is the pressure gradient. The analytical solution of flowrate for a yield-power-law fluid is (see Appendix A),

$$Q = \frac{2Wn}{n+1}\left(-\frac{1}{k}\frac{\partial P}{\partial x}\right)^{\frac{1}{n}} B^{\frac{2n+1}{n}}\left(1 - \frac{z_p}{B}\right)^{\frac{n+1}{n}}\left[1 - \frac{n}{2n+1}\left(1 - \frac{z_p}{B}\right)\right] \tag{5}$$

where the half of the plug flow region z_p can be determined from force balance, written as (Zou et al., 2018)

$$z_p = \tau_0 / \left|\frac{\partial P}{\partial x}\right| \tag{6}$$

According to Eq. (4), the transmissivity for the yield-power-law fluid flow in a homogeneous fracture can be expressed as

$$T = \frac{2WnB^{\frac{2n+1}{n}}}{n+1}\left(\frac{1}{k}\right)^{\frac{1}{n}}\left(-\frac{\partial P}{\partial x}\right)^{\frac{1-n}{n}}\left(1 - \frac{z_p}{B}\right)^{\frac{n+1}{n}}\left[1 - \frac{n}{2n+1}\left(1 - \frac{z_p}{B}\right)\right] \tag{7}$$

For the Bingham fluids, the solution of velocity, flowrate and transmissivity can be obtained directly by equating $n = 1$ in Eqs. (5) and (7) (e.g. Huilgol, 2015). Similarly, equating $z_p = 0$ and further equating $n = 1$ in Eqs. (5) and (7) yields the solution of velocity and flowrate for the power-law fluids and Newtonian fluids, respectively (e.g. Bird et al., 1960). For completeness, the constitutive equations for yield-power-law fluids and derivation of the analytical solutions for the transmissivity are presented in Appendix A.

Eqs. (1)–(3) are a set of coupled nonlinear partial differential equation that defines the mathematical model for the two-phase yield-power-law fluids flow in a fracture. For fracture networks, the solution can be scaled by integration over connected single fractures for each intersection node. The detailed solution method for a fracture network is presented in Appendix B.

3. Experimental verification

To verify the two-phase flow model and the proposed computing algorithm for a fracture network, simulation results are compared with experimental data obtained in a laboratory test system (Fig. 2a) (Håkansson, 1987). The experiment of Håkansson (1987) is considered as a benchmark in the literature (e.g. Hässler, 1991; Eriksson et al., 2000; Mohajerani et al., 2017) mainly because they were conducted on a relatively large scale relevant for fractured rock applications.

This test system consists of two parallel plates of plexiglass with the size of $1.2 \times 1 \times 0.015$ m. The two sides along the length of the plates were sealed and the remaining two sides along the width of the plates

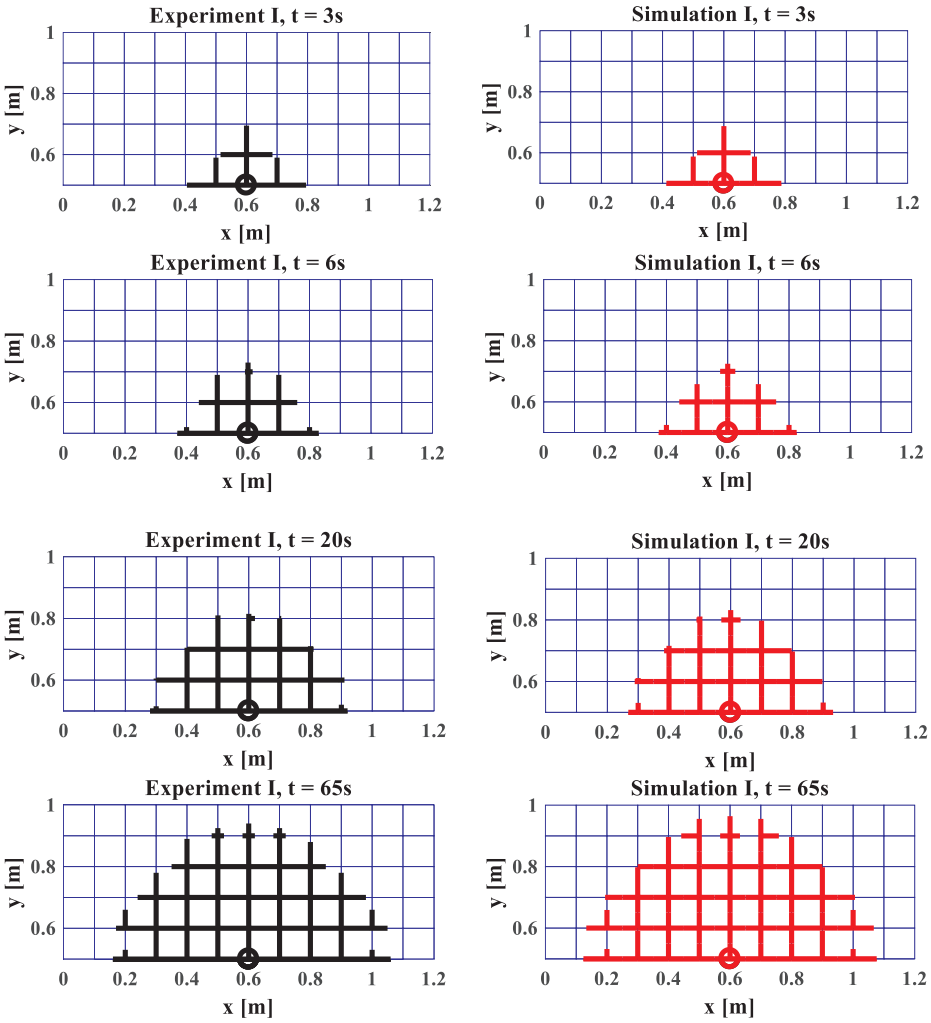

Fig. 3. Comparison of propagation patterns between experiments and simulations at t = 3 s, 6 s, 20 s and 65 s.

were fixed by given water heads. One hundred and twenty rectangular plexiglass plates were homogeneously placed between the two plates to construct the regular fracture network. The fracture aperture is 1 mm and the width of the fractures is 5 mm. At the center of the top plate, a circular hole was drilled for injecting a non-Newtonian fluid.

In this experiment, all fractures were initially filled with water. The injected non-Newtonian fluid was a bentonite grout, characterized by a rheometer and fitted to the Bingham model. The curve fitted yield stress was 3 Pa and the viscosity was 0.035 Pa s; the injected fluid had time constant rheological properties. The injection pressure forcing the fluid displacement was 4.8 kPa and the entire propagation process was filmed by a camera placed orthogonally above the transparent experimental plate. The video of the test, which contains the entire dataset of the propagation time and positions, is presented in the Supplement Material. Specific snapshots from this experiment have been considered in the literature (e.g. Hässler, 1991; Eriksson et al., 2000; Mohajerani et al., 2017), however the full and continuous experimental dataset is presented for the first time in this study.

Using the computational algorithm summarized in Appendix B, we simulated the same fracture system as the laboratory test. Fig. 3 shows comparison of injected fluid propagation in the fracture network for different times, i.e. t = 3 s, 6 s, 20 s and 65 s, between experimental results and numerical simulations. Only the top half of the fracture networks are shown due to symmetry. With increasing time, the injected fluid gradually displaces the water in the fracture network. Simulated result matches very well with the experimental data for all the times. This indicates that the two-phase flow model developed in this study is sufficiently accurate and can be used for modeling two-phase flow of yield-power-law fluids propagation in an advection-dominated, water-saturated fracture network. Compared with the results presented in previous studies (e.g., Hässler, 1991; Eriksson et al., 2000; Mohajerani et al., 2017), simulation results presented in this study (Fig. 3) better match the experimental data, indicating that the mathematical model and solution method are more accurate; further discussion on the advantages of the presented computational methodology in given in Appendix B.

To quantitatively compare and follow the evolution of the propagation process, a parameter representing the volume fraction between the penetrated volume and the total volume of the fractures is defined. Specifically, a propagation volume fraction is

$$\Gamma = \frac{V_p}{V_c} \tag{8}$$

where V_p is the penetrated volume and V_c is the total volume of the fractures. Comparing to traditional measure of grout propagation by penetration length, using the penetration volume has advantages in quantifying the grout propagation in heterogeneous fracture networks and in controlling of the injected volume that is often used as a stop criteria in practice, e.g., Stille (2015).

Fig. 4 shows the evolution of the propagation volume fraction Γ from the numerical simulation result. The experimental result is also presented for comparison, which matches well with the simulation

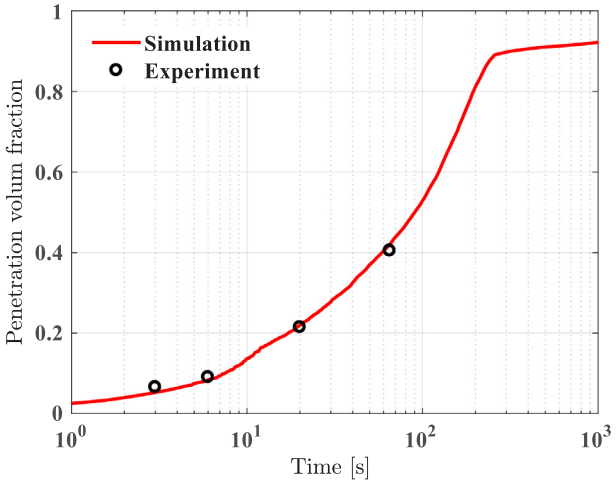

Fig. 4. Comparison of propagation volume fraction between the simulation results and experimental data.

result. The propagation volume fraction Γ increases rapidly in the initial phase and gradually slows down with increasing time, especially after 120 s when the injected fluid arrives at the sealed walls; this is caused by the gradually reduction of the pressure gradient in the fractures and the yield stress of the injected fluid.

4. Illustration examples

4.1. Impact of rheological parameters

In order to investigate the sensitivity of rheological parameters on the propagation, we simulate several cases that vary the parameters in typical ranges. To be representative, the ranges of the varying parameters are chosen from the physical properties of cement grouts that are typical yield-power-law fluids (Håkansson et al., 1992; Nguyen et al., 2006; Rahman et al., 2015). Specifically, the cases for yield stress $\tau_0 = 0.5$ Pa, 2.5 Pa and 5 Pa, k = 1, 1.5 and 2, and n = 0.4, 0.45 and 0.5, are considered. The injection pressure is 4.8 kPa and the fracture model and boundary conditions are identical to the experiment in Fig. 2 for all simulations in this section.

Fig. 5 presents the evolution of the propagation volume fraction for different values of the yield stress $\tau_0 = 0.5$ Pa, 2.5 Pa and 5 Pa, where k = 1.5 and n = 0.4. When the yield stress is relatively small, i.e. $\tau_0 = 0.5$ Pa, the propagation volume fraction increases relatively fast until the fracture network is filled with the injected yield-power-law fluid. The rate of the propagation volume fraction reduces dramatically when the yield stress increases. Particularly, when the yields stress is $\tau_0 = 5$ Pa, the propagation volume fraction approaches the maximum value of around 0.42, which is much smaller than in the case with $\tau_0 = 0.5$ Pa. This indicates that the yield stress significantly affects the propagation of a yield-power-law fluid in a fracture network, because it determines the transmissivity and thereby controls the propagation (Gustafson et al., 2013; Zou et al., 2018).

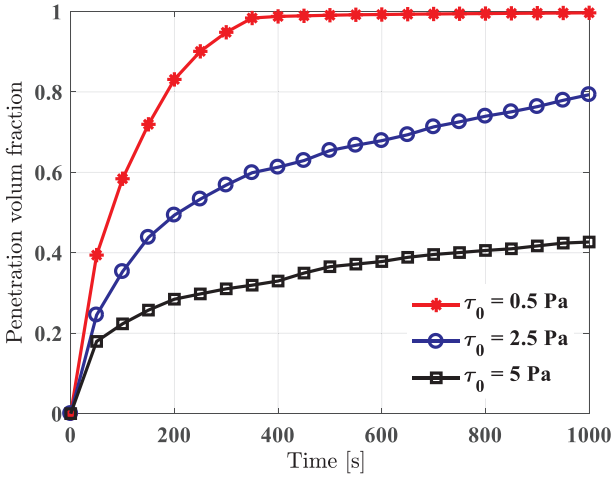

Fig. 5. Comparison of the propagation volume fraction Γ Eq. (8) for different values of the yield stress $\tau_0 = 0.5$ Pa, 2.5 Pa and 5 Pa, where k = 1.5 and n = 0.4.

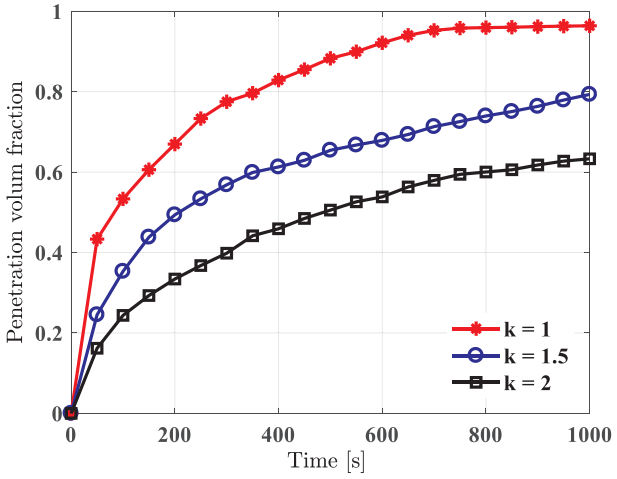

Fig. 6. Comparison of the propagation volume fraction Γ Eq. (8) for different values of k, where $\tau_0 = 2.5$ Pa and n = 0.4.

Fig. 6 shows the evolution of the propagation volume fraction Γ for different values of the consistency index k = 1, 1.5 and 2, where $\tau_0 = 2.5$ Pa and n = 0.4. After injection, the case with smaller consistency index k generally has a higher propagation volume fraction. The propagation rate reduces with increasing k values from 1 to 2. This result illustrates that the rate of propagation volume fraction is also sensitive to the consistency index k.

Fig. 7 presents the evolution of the propagation volume fraction for different values of the flow index n = 0.4, 0.45 and 0.5, where $\tau_0 = 2.5$ Pa and k = 1.5. The rate of propagation volume fraction reduces with increasing flow index n from 0.4 to 0.5, indicating that the flow index n also influences the propagation process.

To summarize, the propagation of yield-power-law fluids in water saturated fracture networks is sensitive to the rheological parameters.

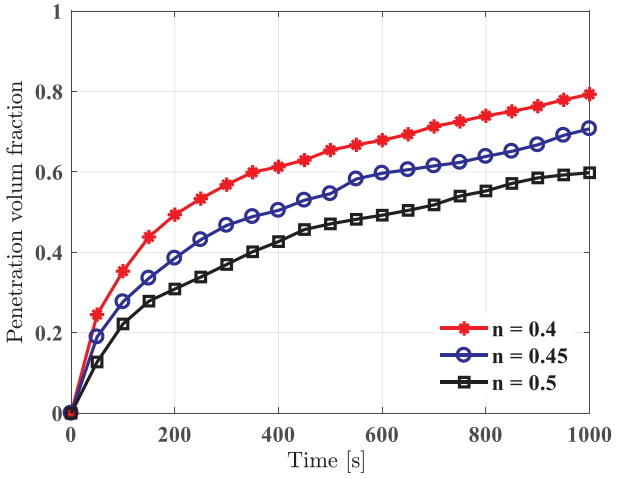

Fig. 7. Comparison of the propagation volume fraction Γ Eq. (8) for different values of n, where $\tau_0 = 2.5$ Pa and k = 1.5.

The maximum propagation volume fraction reduces with increase of the yield stress. The propagation rate increases with the decrease of the consistency index and the flow index. In order to predict the propagation volume fraction in applications, the constitutive properties of the yield-power-law fluids should be determined with high accuracy.

4.2. Impact of time-dependent rheological properties

In engineering applications, rheological properties of many non-Newtonian fluids will change over time. For instance, cement grouts will harden where the yield stress and viscosity increase with time due to both physical and chemical processes. It is therefore of interest to illustrate the impact of the time-dependent rheological properties. Håkansson (1993) and Hässler (1991) used linear functions and exponential functions to model the hardening process for cement/bentonite grouts. Subramaniam and Wang (2010) found that the shear modulus and yield stress of the cement paste increase rapidly with time, almost exponential in the initial period. Fidelibus and Lenti (2012) used an exponential function to model the increase of grout viscosity with time. Rahman et al., (2015) found that the yield stress and consistency index of the cement grouts generally increases with time while the flow index is comparatively less sensitive. The exponential function is also adopted in this study to describe time-dependent yield stress and consistency index of the injected yield-power-law fluids, written as,

$$\tau_0(t) = \tau_I e^{bt} \tag{9}$$

$$k(t) = k_I e^{at} \tag{10}$$

where τ_I and k_I is the initial yield stress and consistency index respectively, while a and b are parameters controlling the rate of increase (i.e., hardening rate). The hardening model based on the exponential functions (9)–(10) is valid only for the initial period, which is relevant for most of geo-engineering applications, because the injection time is often relatively short and within the initial period of hardening.

The initial yield stress $\tau_I = 2.5$ Pa and initial consistency index $k_I = 1.5$ are adopted here for simulation. To illustrate the sensitivity, two sets of parameter a and b, representing low ($a = b = 0.0005$) and high ($a = b = 0.001$) hardening rate are simulated and compared with the time constant case with $\tau_0 = \tau_I = 2.5$ Pa and $k = k_I = 1.5$, i.e. $a = b = 0$. Fig. 8 presents the comparison of propagation volume fraction for the time constant and time-dependent cases with flow index $n = 0.4$.

Comparing the evolution of propagation volume fraction with the time constant case, both the propagation rate and the maximum of propagation volume fraction reduces significantly with the time-dependent rheological properties. More specifically, the case with higher hardening rate, i.e. a = b = 0.001, has slower propagation rate and smaller propagation volume fraction than the case with lower hardening rate, i.e. a = b = 0.0005. This result indicates that it is important to consider the more realistic time-dependent rheological properties in the modeling of yield-power-law fluids propagation in fracture networks. Simplifications without consideration of the time-dependent rheological properties may imply considerable uncertainty in prediction of the propagation process.

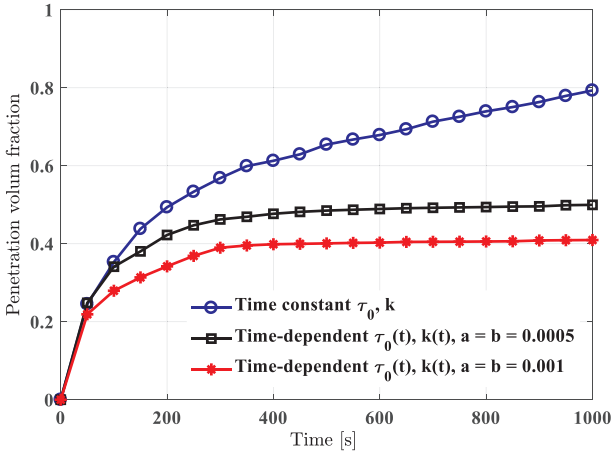

Fig. 8. Comparison of the propagation volume fraction Γ (Equation (8)) for the constant and time-dependent yield stress and consistency index, where $\tau_0 = \tau_I = 2.5$ Pa, k = k_I = 1.5 and $n = 0.4$.

5. Heterogeneous fracture networks

Hydraulic properties of geological media are heterogeneous on a wide range of scales. A variety of models have been used to represent this heterogeneity, from continuum to discrete, from one-dimensional to three-dimensional (Baghbanan and Jing, 2007; Cvetkovic and Frampton, 2012; Dessirier et al., 2018). The fracture network model could be assigned different distribution of apertures, where for instance log-normal or fractal models have been used to represent aperture distributions (e.g. Wang et al., 1988; Gustafson and Fransson, 2005; Baghbanan and Jing, 2007; Cvetkovic and Frampton, 2012). In this section, we choose to investigate the impact of heterogeneity on the propagation of yield-power-law fluid in a heterogeneous fracture network by assuming the simplest two-point distribution for the random aperture. Specifically, the probability of the aperture b in the network is expressed as

$$f(b; p) = \begin{cases} pifb = b_1 \\ 1 - pifb = b_2 \end{cases} \tag{11}$$

where p is the probability that the aperture is b_1, and $1 - p$is the probability that the aperture is b_2. In the simulation, the size of the fracture network is1m × 1m, roughly the same size as the experimental setup of Fig. 2. The length of each fracture is 0.05 m and the width of fracture is 5 mm. The two values of the aperture are b_1 = 1mm and b_2 = 0.5mm. Consistent with the experimental conditions of Section 3 and the constitutive parameters considered in Section 4, the injection pressure is 4.8 kPa, with four simulated cases: (a) Newtonian fluid (water), τ_0 = 0 Pa, k= 0.001 and n = 1; (b) Power-law fluid, τ_0 = 0 Pa, k= 1.5 and n = 0.4; (c) Bingham fluid, τ_0 = 2.5 Pa, k= 1.5 and n = 1; and (d) Herschel-Bulkley fluid, τ_0 = 2.5 Pa, k= 1.5 and n = 0.4, respectively. With these simulations, varying the heterogeneity probability p will enable us to illustrate the combined effect of heterogeneity and the rheological parameters. Our particular interest is to see whether a consistent effective aperture representation is possible.

Fig. 9 shows two examples of propagation patterns at t = 30 s and 1000 s, for the case of Herschel-Bulkley fluid with p = 0.5. The thicker lines represent fracture apertureb_1 = 1 mm. The propagation of Herschel-Bulkley fluid (in red color) has preference for fractures with the larger apertureb_1 = 1 mm at the beginning (Fig. 9a), due to its corresponding higher transmissivity values, which yields an asymmetric propagation front. However, at longer time or larger scale, the propagation front becomes asymptotically symmetric because the heterogeneity of structures is scale-dependent.

Fig. 10 shows the propagation volume fraction curves for different p values (p = 0, 0.25, 0.5, 0.75 and 1), where p = 0 and 1 are the two extreme cases with homogeneous apertures 0.5 mm and 1 mm, respectively. For each heterogeneous case (p = 0.25, 0.5 and 0.75), 20 realizations were computed; the propagation volume fraction curves presented in Fig. 10 is the mean of 20 realizations. The error bars represent standard deviations.

For all simulations with four different fluids, the propagation volume fraction for cases p = 1, b = 1 mm are much larger than that of cases p = 0, b = 0.5 mm. Meanwhile, propagation volume fraction nonlinearly reduces with the decrease of p from 1 to 0 in all cases, indicating that the propagation process significantly depends on the

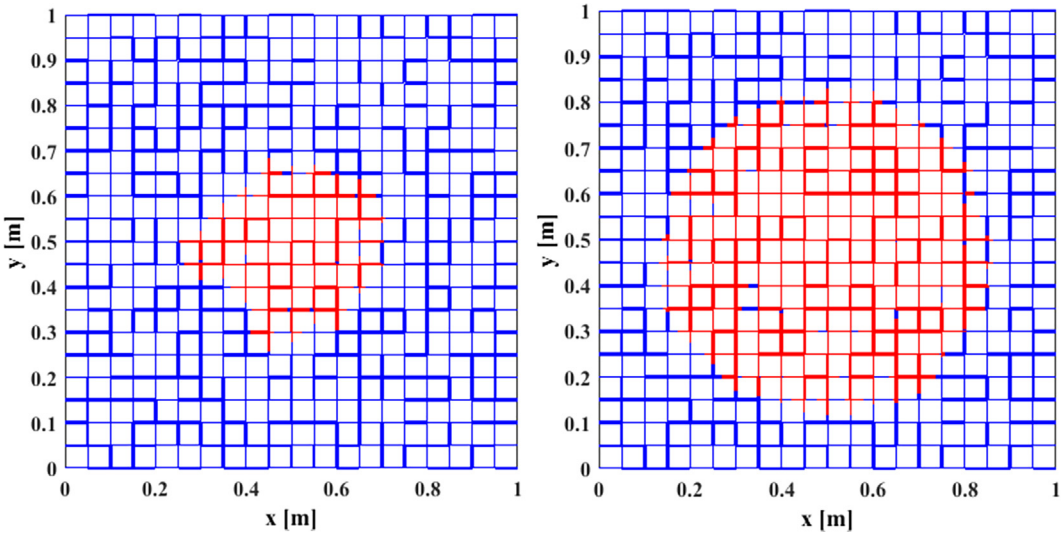

Fig. 9. An example of propagation patterns in a fracture network with heterogeneous apertures for p = 0.5, (a) t = 30 s and (b) t = 1000 s. The bold fractures represent $b_1 = 1$ mm.

values of fracture aperture. The error bars (standard derivations) for the cases p = 0.25, 0.5 and 0.75 represent uncertainty of the propagation volume fraction which slightly increases with the increase of p. Such uncertainty is caused by the spatial heterogeneity of aperture distributions.

For upscaling of the heterogeneous networks, it is of interest to determine the effective homogeneous aperture. We compared the upscaling results using the harmonic mean of the heterogeneous apertures for the four fluids shown in Fig. 10. For the two-point distribution, the harmonic mean is

$$b_{hm} = \frac{b_1 b_2}{(1-p)b_1 + pb_2} \tag{12}$$

The result shows that the propagation volume fraction for the heterogeneous aperture cases with two-point distributions can be approximated through upscaling using the harmonic mean aperture.

6. Discussion

A two-phase flow model for the general yield-power-law fluid flow in randomized fractures is presented using the methodology we originally developed for Bingham fluids (Zou et al., 2018). The more general yield-power-law rheological model covers a broad range of non-Newtonian fluids that commonly appears in rock grouting applications (Nguyen et al., 2006; Funehag and Fransson, 2006; Rahman et al., 2015; Pedrotti et al., 2017; Liang et al., 2019). The mathematical model for the two-phase flow extended in this study is based on the assumption that the two phases are immiscible. This assumption implies that the propagation of yield-power law fluid is a pure advective process. To resolve the advection problem, a Lagrangian method with a moving node in each fracture to track the interface is proposed. The moving node method can also be used to solve general two-phase advective flow. The experimental results confirm that the propagation process is generally dominated by advection with relatively sharp interfaces at propagation fronts (see Supplement Material). In geoengineering applications however, the injected fluids, e.g. cement grouts, may slightly mix with the groundwater (Hässler 1991), especially at the fracture intersections (Zou et al., 2017a). For specific applications, the validity of this assumption and the impact of potential mixing behavior need to be further studied both by laboratory experiments and direct numerical simulations.

The simulation results presented in this study are based on a relatively simple geometrical model, i.e., the smooth parallel plate model without consideration of any internal heterogeneity such as surface roughness, and the simplest regular fracture networks. In applications, the geometrical structure of rock fractures often consists of rough surfaces (e.g., Brown, 1987; Roustaei and Frigaard, 2013; Zou et al., 2015; 2017b), and the rock fracture networks are mostly random (e.g., Cacas et al., 1990; Baghbanan and Jing, 2007; Cvetkovic and Frampton, 2012). These complex geometrical structures may cause complex flow behaviors (e.g., Brown, 1987; Zou et al., 2015, 2017b; Ju et al., 2017; Jin et al., 2019). However, direct simulation of yield fluid flow in realistic rough-walled fracture remains a challenge due to discontinuity caused by the yield stress (Roustaei and Frigaard, 2013; Balmforth et al., 2014; Saramito and Wachs, 2017). Quantifying the impact of these complex geometrical structures on grouts propagation in more realistic rock fractures and networks remains an open issue that needs to be further studied in the future.

We only studied the simplest case for the randomized fracture aperture that follows the two-point distribution. In reality, the fracture aperture may follow other statistical distributions, e.g., lognormal, or correlated with the fracture size (e.g. Wang et al., 1988; Eriksson et al., 2000; Gustafson and Fransson, 2005; Baghbanan and Jing, 2007; Cvetkovic and Frampton, 2012; Zhao et al., 2013, 2014). These geometrical conditions can cause potentially important uncertainties in prediction of the propagation process in applications, and are therefore important topics for further studies. Nevertheless, the mathematical model developed in this work constitutes a sound basis that can be further extended to consider such uncertainties.

The impact of the rheological properties of yield-power-law fluids is illustrated by sensitivity analyses, i.e., by varying the parameters, in particular the yield stress, flow and consistency indices. The ranges of these parameters are chosen according to typical yield-power-law fluids used in geoengineering, such as cement grouts (Nguyen et al., 2006; Rahman et al., 2015). Therefore, the results of the sensitivity analyses shown in Figs. 5–8 may be useful for the design of rock grouting. In such applications, it is important to consider time/space-dependent and even temperature-dependent rheological properties of the injected fluids, since they may significantly affect the propagation processes (e.g., Fidelibus and Lenti 2012; Rahman et al., 2015; Zhang et al., 2017; Liang et al., 2019; Bohloli et al., 2019).

To face the engineering challenges of cement grouting for subsurface formations, reliable and accurate measurements of the rheological parameters, and advanced laboratory experiments as well as field tests for verifying the effects of rheological properties and geometry conditions on the propagation process are needed. Laboratory experiments

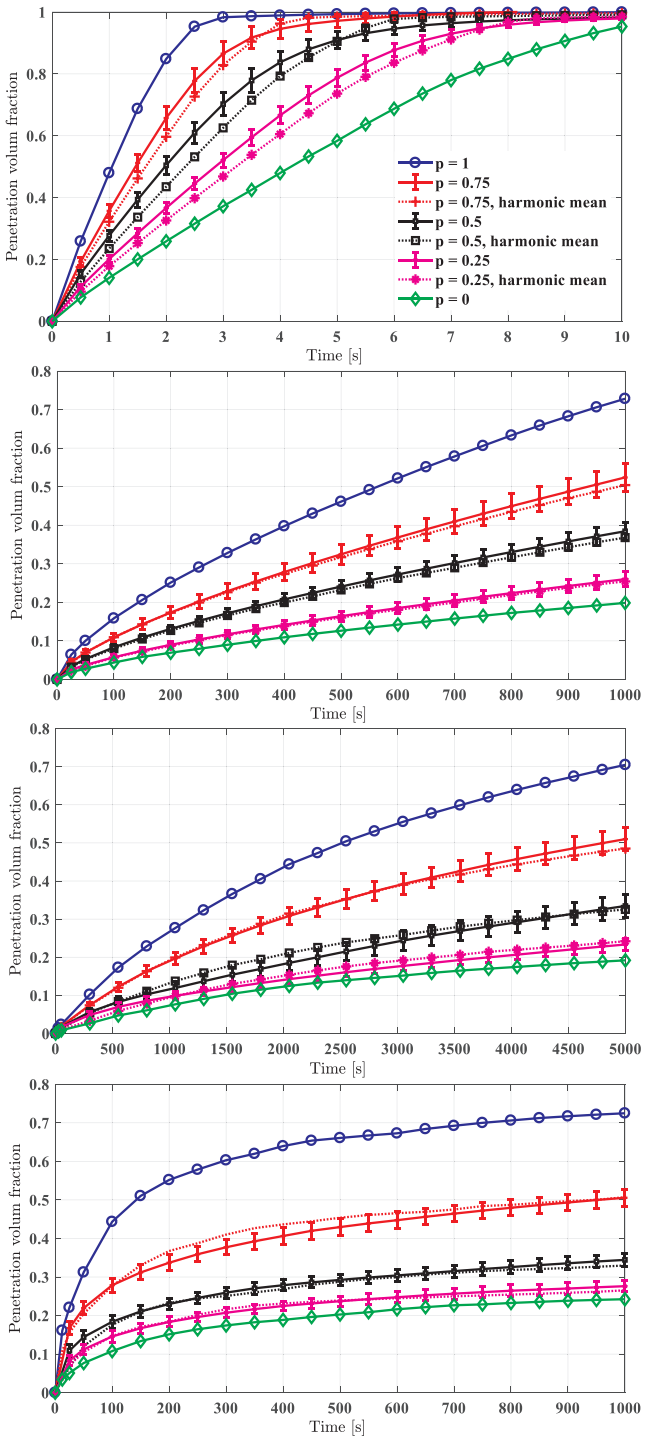

Fig. 10. Propagation volume fraction curves for different p values (p = 0, 0.25, 0.5, 0.75 and 1), (a) Newtonian fluid (water), τ_0 = 0 Pa, k= 0.001 and n = 1; (b) Power-law fluid, τ_0 = 0 Pa, k= 1.5 and n = 0.4; (c) Bingham fluid, τ_0 = 2.5 Pa, k= 1.5 and n = 1; and (d) Herschel-Bulkley fluid, τ_0 = 2.5 Pa, k= 1.5 and n = 0.4. The dashed lines represent scaling of corresponding heterogeneous cases using the harmonic mean aperture Eq. (12).

on propagation of cement grouts in a single fracture with variable apertures and ultrasound sensors have been designed and applied in tests recently (e.g. Ghafar et al., 2017; Rahman et al., 2015; Funehag and Thörn, 2018; Liang et al., 2019; Xu et al., 2019). Comparisons between modeling results and these experimental data could be important tasks for future studies.

7. Conclusions

In this work, we extended the two-phase flow model for a Bingham fluid in a single fracture presented in Zou et al. (2018) to yield-power-law fluids in a network of fractures. Using the extended model, we studied the propagation of yield-power-law fluids in water-saturated regular and randomized fracture networks, which is an important topic in modeling of cement grouting in fractured rocks. The most important conclusions from this study are summarized as follows:

- The extended two-phase flow model for fracture networks is verified using benchmark experimental data. Simulation results have been found to match closely to the observations. The extended model provides an accurate and efficient numerical tool for modeling advection-dominated two-phase flow of yield-power-law fluids propagation in water-saturated, randomized fracture networks, which can be used for rock grouting design.
- The propagation process in fracture networks can be quantitatively described by the propagation volume fraction that has been defined in equation (8). The evolution of propagation volume fraction is sensitive to the rheological parameters of the injected yield-power-law fluid. The propagation rate reduces with increase of the yield stressτ_0, the consistency index k and the flow index n. The maximum propagation volume fraction also decreases with the increase of yield stress τ_0.
- The time-dependent rheological properties (i.e., the hardening process) significantly affect the propagation process. Ignoring the time-dependent rheological properties will largely overestimate the predicted propagation volume fraction in practice. When the hardening rate is relatively high, i.e., a = b = 0.001, the maximum propagation volume fraction (Γ = 0.4) reduces to 50% of the case without consideration of hardening (Γ = 0.8). Similarly, even when the hardening rate is relatively low, i.e., a = b = 0.0005, the maximum propagation volume fraction (Γ = 0.5) reduces to62.5% of the case without consideration of hardening (Γ = 0.8).
- The heterogeneity of fracture aperture with randomized two-point distribution yields an uncertain propagation volume fraction. The propagation volume fraction generally reduces with a decreasing fraction (p) of the larger aperture.
- The two-phase flow of yield-power-law fluids in randomized fracture networks with two-point aperture distribution can be well represented by the harmonic mean aperture, which provides an effective aperture for upscaling analysis.

In practice, rock grouting involves complex fluids propagation in complex fracture networks. The complex rheological properties of grouts and the complex geometrical structures of the rock fracture networks cause major challenges and significant uncertainties for modeling of rock grouting in applications. Extension of the mathematical model to account for the more realistic rheological properties of gouts and geometrical structures of natural rock fracture networks, and to compare with high-quality experimental results are important tasks for future studies.

Declaration of Competing Interest

The authors declare that they have no known competing financial interests or personal relationships that could have appeared to influence the work reported in this paper.

Acknowledgements

This study is funded by the BeFo Rock Engineering Research Foundation, which is thankfully acknowledged.

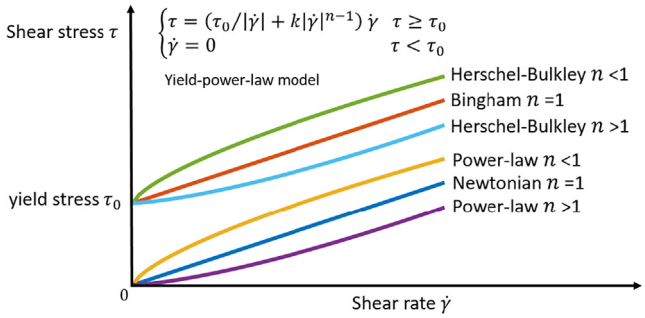

Fig. A1. Illustration of rheological models for yield-power-law fluids.

Appendix A. Analytical solution for yield-power-law fluid flow between parallel plates

The yield-power-law model is a generalized rheological model for non-Newtonian fluids, which is illustrated by Fig. A1. By specifying controlling parameters, the yield-power-law model can be classified into four categories as follows (Herschel and Bulkley, 1926; Mitsoulis, 2007):

(1) *Herschel-Bulkley model*. The constitutive equation of the Herschel-Bulkley model for the general yield-power-law fluids can be mathematically expressed as

$$\begin{cases} \tau = (\tau_0/|\dot{\gamma}| + k\,|\dot{\gamma}|^{n-1})\dot{\gamma},\ \tau \geq \tau_0 \\ \dot{\gamma} = 0 \tau < \tau_0 \end{cases} \tag{A1}$$

where τ is the shear stress, τ_0 is the yield stress, k is the consistency index, n is the power-law index, and$\dot{\gamma}$ is the shear rate.

(2) *Bingham model*. By taking the power-law exponent $n = 1$, the Herschel-Bulkley model reverts to the Bingham model, written as

$$\begin{cases} \tau = (\tau_0/|\dot{\gamma}| + k)\dot{\gamma},\ \tau \geq \tau_0 \\ \dot{\gamma} = 0 \tau < \tau_0 \end{cases} \tag{A2}$$

In this case, the consistency index k is the plastic viscosity.

(3) *Power-law model*. When the yield stress$\tau_0 = 0$, the Herschel-Bulkley model transfers into the power-law model, expressed by

$$\tau = (k\,|\dot{\gamma}|^{n-1})\dot{\gamma} \tag{A3}$$

(4) *Newtonian model*. When both the yield stress$\tau_0 = 0$ and the power-law index $n = 1$, the Herschel-Bulkley model reduces to the Newtonian model, expressed as

$$\tau = k\dot{\gamma} \tag{A4}$$

In this case, the consistency index k is the dynamic viscosity.

By invoking the assumptions summarized in Section 2, the governing equation for a single-phase yield-power-law fluid flow in parallel plates can be written as (Bird et al., 1960)

$$\frac{\partial P}{\partial x} + \frac{\partial \tau_{zx}}{\partial z} = 0 \tag{A5}$$

The boundary conditions are

$$P(x = 0) = P_1,\ P(x = L) = P_2 \tag{A6}$$

$$v_x(z = \pm B) = 0 \tag{A7}$$

$$\frac{\partial v_x}{\partial z}(r, z = \pm z_p) = 0 \tag{A8}$$

where z_p is half of the plug flow region caused by the yield stress and B = b/2 is the half of the fracture aperture. Eq. (A6) represents the known pressure boundary conditions; Eq. (A7) denotes no-slip boundary condition on the plate walls, and Eq. (A8) represents the no-shear rate condition in the plug flow region for yield-stress fluids, i.e. Herschel-Bulkley and Bingham fluids.

The integration of the pressure term in Eq. (A5), after introducing the pressure boundary condition, yields

$$P = -\frac{(P_1 - P_2)}{L}x + P_0 \tag{A9}$$

$$\frac{\partial P}{\partial x} = -\frac{(P_1 - P_2)}{L} \tag{A10}$$

The integration of the shear stress in Eq. (A5) then gives,

$$\tau_{zx} = \tau_0 - \frac{\partial P}{\partial x}(z - z_p) \tag{A11}$$

The solution of velocity is an even function of$z$. For the upper half aperture, $z_p \leq z \leq B$, invoking Eq. (A11) into Eq. (A5) gives

$$-\frac{\partial P}{\partial x}(z-z_p)=k\left(-\frac{\partial v_x}{\partial z}\right)^n \tag{A12}$$

The velocity can now be obtained by introducing the no-slip boundary condition after integration of Eq. (A12) over z:

$$v_x(z_p<z\le B)=\frac{n}{n+1}\left(-\frac{1}{k}\frac{\partial P}{\partial x}\right)^{\frac{1}{n}}\left[(B-z_p)^{\frac{n+1}{n}}-(z-z_p)^{\frac{n+1}{n}}\right] \tag{A13}$$

$$v_x(0\le z<z_p)=\frac{n}{n+1}\left(-\frac{1}{k}\frac{\partial P}{\partial x}\right)^{\frac{1}{n}}(B-z_p)^{\frac{n+1}{n}} \tag{A14}$$

Integration of the velocity over the aperture across z-axis gives

$$Q=2W\int_0^B v_x dz \tag{A15}$$

where Q is flowrate that can be obtained as defined in Eq. (5).

Appendix B. Solution method for advection-dominated two-phase yield-power-law fluid flow in fracture works

The governing equations of the two-phase flow model (1)–(3) are a set of nonlinear Reynolds equations coupled with the interface transport equation. The Picard iterative method is used to solve the nonlinear Reynolds Eq. (1) and the interface transport Eq. (3). At each time step, the velocity is calculated by Eq. (2) after obtaining a convergent pressure field.

A finite volume method (FVM) is implemented to solve the nonlinear Reynolds equation. The FVM is used because of its advantages in securing mass balance and flexibility in consideration of complex geometry and spatially varying properties of the non-Newtonian fluids. It is based on the integration form of the Reynolds equation, expressed as

$$\int \frac{\partial}{\partial \mathrm{x}}T(C)\frac{\partial \mathrm{P}}{\partial \mathrm{x}}dx=\sum T(C)\frac{\partial P}{\partial \mathrm{x}}=0 \tag{B1}$$

Fig. B1 illustrates an intersection within the fracture network. The integration form of the Reynolds Eq. (B1) represents the mass balance at each node.

For any node i in the lattice model (Fig. B1), Eq. (B1) can be discretized as

$$\sum_{j=1}^{M}[T(C)]_{ij}\frac{P_j-P_i}{L_{ij}}=0 \tag{B2}$$

where M is the number of neighboring nodes, and L_{ij} is the length between the nodes i and j. Assembling the discretized Eq. (B2) over all cells yields a system of linear equations, which are solved by using a direct solver, such as Cholesky factorization.

The phase transport is a hyperbolic (advection) equation, which is a difficult numerical problem in the presence of a sharp interface (i.e., high phase gradient) at the propagation front if an Eulerian scheme is used. To overcome this numerical difficulty, a Lagrangian interface tracking method was adopted to track the grout propagation, which can be written as (Zou et al., 2018)

$$\mathrm{I}^{n+1}=\mathrm{I}^{n}+\mathrm{u}(\mathrm{I}^{n})\Delta \mathrm{t} \tag{B3}$$

whereI is the position of the interface and Δt is the time step. Since equation (B3) is an explicit discretization scheme, the adaptive time step based on the Courant-Friedrichs-Lewy (CFL) condition is used in this study to achieve higher efficiency and maintain computational stability for the solution, expressed by

$$\Delta \mathrm{t}\le\frac{\Delta \mathrm{x}}{\mathrm{u}} \tag{B4}$$

where Δx is a characteristic length assumed to be the minimum volume/cell length. In networks, it also should avoid discontinuity at intersections,

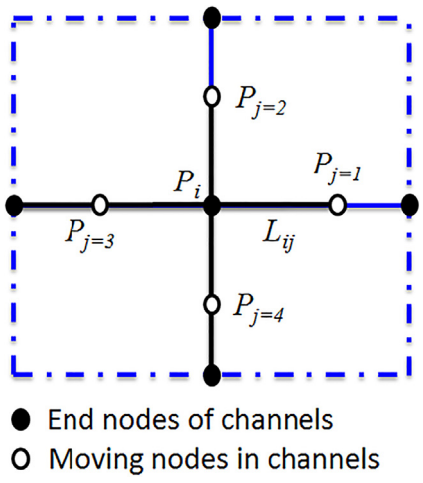

Fig. B1. Illustration of the solution method for fracture networks.

which requires

$$\Delta t \le \frac{\Delta L}{u} \tag{B5}$$

whereΔL is the minimum distance to the closest intersection. Therefore, the final adaptive time step is

$$\Delta t = \min\left(\frac{\Delta x}{u}, \frac{\Delta L}{u}\right) \tag{B6}$$

To implement the particle tracking, we add a moving node in each single fracture to represent the propagation of the propagation fronts/interfaces (Fig. B1). This method overcomes the difficulty in determining transmissivity for the fracture that contains the interface. When the fracture is filled with a single-phase fluid, i.e. the yield-power-law fluid or water, the node is placed in the middle of the fracture. This middle node adds to the computational load since the number of computing volumes/cells is doubled, but it simplifies the programming considerably, since the connectivity geometry and data structure remains constant even though the volume sizes changes due to the propagation of the propagation interfaces.

Using this solution strategy, we directly solve the Reynolds equation by FVM and use the particle tracking method to capture the interface. This introduces a moving mesh due to the interface propagation, but it avoids any iteration for solving the pressure at the propagation interfaces in partially filled fractures. The detailed algorithm of the two-phase flow solver for modeling of yield-power-law fluids propagation in water-saturated fracture networks is summarized as follows (Zou et al., 2019):

(a) Define rheological parameters, controlling parameters and geometry model, including fracture nodes and connections.
(b) Initialize the phase function C and pressure field P_0 for t = 0.
(c) Determine the effective transmissivity $T(C)$.
(d) Compute the pressure $P_1$by solving Eq. (B2).
(e) Compare pressure P_1 with previous pressure field P_0: if the differences meet the convergence condition $|P_1 - P_0| < \varepsilon$, then go to (f); otherwise, $P_0 = P_1$ go back to (c).
(f) Compute the velocity u and determine the time stepΔt based on Eq. (B6).
(g) Update the phase function C, i.e. update the location of interface through particle tracking based on Eq. (B3), and t = t $+\Delta t$.
(h) Stop criteria: if $t < t_{max}$, go back to (c); otherwise, stop.

An alternative approach for resolving the two-phase flow in fracture networks can be found in the literature for the Bingham fluid, e.g., Hässler (1991), Fidelibus and Lenti (2012). In their method, the flowrate equation and the interface pressure is iteratively solved from an implicit equation, which adds a significant computational burden as convergence may take prohibitively long time. In contrast, we introduced a moving interface node to explicitly track the interface; the interface pressure can thereby be solved in a straightforward manner without necessity of extra iterations.

Appendix C. Supplementary material

Supplementary data to this article can be found online at https://doi.org/10.1016/j.tust.2019.103170.

References

Baghbanan, A., Jing, L., 2007. Hydraulic properties of fractured rock masses with correlated fracture length and aperture. Int. J. Rock Mech. Min. Sci. 44 (5), 704–719.

Balhoff, M., Sanchez-Rivera, D., Kwok, A., et al., 2012. Numerical algorithms for network modeling of yield stress and other non-Newtonian fluids in porous media. Transp. Porous Med. 93, 363. https://doi.org/10.1007/s11242-012-9956-5.

Balmforth, Neil J., Frigaard, Ian A., Ovarlez, Guillaume, 2014. Yielding to stress: recent developments in viscoplastic fluid mechanics. Annu. Rev. Fluid Mech. 46 (1), 121–146.

Bird, R.B., Stewart, W., Lightfoot, E., 1960. Transport Phenomena. John Wiley & Sons, New York.

Bohloli, Bahman, Skjølsvold, Ola, Justnes, Harald, Olsson, Roger, Grøv, Eivind, Aarset, Arnstein, 2019. Cements for tunnel grouting – rheology and flow properties tested at different temperatures. Tunnel. Undergr. Space Technol. 91, 103011. https://doi.org/10.1016/j.tust.2019.103011. ISSN 0886-7798.

Brown, S.R., 1987. Fluid flow through rock joints: the effect of surface roughness. J. Geophys. Res. 92 (B2), 1337–1347. https://doi.org/10.1029/JB092iB02p01337.

Butrón, C., Axelsson, M., Gustafson, G., 2009. Silica sol for rock grouting: laboratory testing of strength, fracture behaviour and hydraulic conductivity. Tunn. Undergr. Space Technol. 24, 603–607.

Cacas, M.C., Ledoux, E., Marsily, G., Tillie, B., Barbreau, A., Durand, E., Feuga, B., Peaudecerf, P., 1990. Modeling fracture flow with a stochastic discrete fracture network: calibration and validation: 1. The flow model. Water Resour. Res. 26 (3), 479–489. https://doi.org/10.1029/WR026i003p00479.

Cvetkovic, V., Frampton, A., 2012. Solute transport and retention in three-dimensional fracture networks. Water Resour. Res. 48 (2), W02509. https://doi.org/10.1029/2011WR011086.

Deng, S., Wang, X., Yu, J., et al., 1801. Simulation of grouting process in rock masses under a dam foundation characterized by a 3D fracture network. Rock Mech. Rock Eng. 51. https://doi.org/10.1007/s00603-018-1436-y.

Dershowitz, W., Shuttle, D., Lee, G., Rogers, S., 2007. 2007, analysis of groundwater inflow control by grouting using the discrete fracture network method. Felsbau 25 (4), 34–41.

Dessirier, B., Tsang, C.F., Niemi, A., 2018. A new scripting library for modeling flow and transport in fractured rock with channel networks. Comput. Geosci. 111, 181–189.

Dreuzy, J.-R., Méheust, Y., Pichot, G., 2012. Influence of fracture scale heterogeneity on the flow properties of three-dimensional discrete fracture networks (DFN). J. Geophys. Res. 117, B11207. https://doi.org/10.1029/2012JB009461.

El Tani, M., 2012. Grouting rock fractures with cement grout. Rock Mech. Rock Eng. 45, 547–561. https://doi.org/10.1007/s00603-012-0235-0.

Emmelin, A., Brantberger, M., Eriksson, M., Gustafson, G., Stille, H., 2007. Rock grouting: current competence and development for the final repository, SKB Report, R-07-30.

Eriksson, M., Stille, H., Andersson, J., 2000. Numerical calculations for prediction of grout spread with account for filtration and varying aperture. Tunn. Undergr. Space Technol. 15 (4), 353–364.

Fidelibus, C., Lenti, V., 2012. The propagation of grout in pipe networks. Comput. Geosci. 45, 331–336.

Frigaard, I.A., Paso, K.G., de Souza Mendes, P.R., 2017. Bingham's model in the oil and gas industry. Rheol Acta 56, 259. https://doi.org/10.1007/s00397-017-0999-y.

Funehag, J., Fransson, Å., 2006. Sealing narrow fractures with a Newtonian fluid: model prediction for grouting verified by field study. Tunn. Undergr. Space Technol. 21 (5), 492–498.

Funehag, Johan, Thörn, Johan, 2018. Radial penetration of cementitious grout – laboratory verification of grout spread in a fracture model. Tunn. Undergr. Space Technol. 72 (2018), 228–232.

Ghafar, A., Sadrizadeh, S., Magakis, K., Draganovic, A., Larsson, S., 2017. Varying aperture long slot (VALS), a method for studying grout penetrability into fractured hard rock. Geotech. Test. J. 40 (5), 871–882.

Gustafson, G., Claesson, J., Fransson, Å., 2013. Steering parameters for rock grouting. J. Appl. Math. https://doi.org/10.1155/2013/269594.

Gustafson, G., Fransson, Å., 2005. The use of the Pareto distribution for fracture transmissivity assessment. Hydrogeol. J. 14, 15–20.

Herschel, W.H., Bulkley, 1926. R. Kolloid-Zeitschrift 39, 291. doi: 10.1007/BF01432034.

Huilgol, R.R., 2015. Fluid Mechanics of Viscoplasticity. Springer-Verlag, Berlin Heidelberg.

Hässler, L., Håkansson, U., Stille, H., 1992. Computer-simulated flow of gorut in jointed rock. Tunnel. Undergr. Space Technol. 7 (4), 441–446.

Hässler L., 1991 Grouting of Rock—Simulation and Classification. Ph.D. Thesis, Dept. of Soil and Rock Mechanics, Royal Institute of Technology, Stockholm, Sweden.

Håkansson, U., Hässler, L., Stille, H., 1992. Rheological properties of microfine cement grout. Tunnel. Undergr. Space Technol. 7 (4), 453–458.

Håkansson, U., 1993. Rheology of Fresh Cement Based Grouts. PhD Thesis, Royal Institute

of Technology.
Håkansson, U. 1987. Modellförsök – Icke-Newtonsk strömning i endimensionella kanaler. [Master Thesis]. Department of Civil and Environmental Engineering, KTH Royal Institute of Technology, Stockholm, Sweden.
Jin, L., Sui, W., Xiong, J., 2019. Experimental investigation on chemical grouting in a permeated fracture replica with different roughness. Appl. Sci. 9 (13), 2762.
Ju, Y., et al., 2017. Fractal model and Lattice Boltzmann method for characterization of non-Darcy flow in rough fractures. Sci. Rep. 7, 41380.
Li, Shucai, Liu, Rentai, Zhang, Qingsong, Zhang, Xiao, 2016. Protection against water or mud inrush in tunnels by grouting: a review. J. Rock Mech. Geotech. Eng. 8 (5), 753–766.
Liang, Yankun, Sui, Wanghua, Qi, Jianfeng, 2019. Experimental investigation on chemical grouting of inclined fracture to control sand and water flow. Tunn. Undergr. Space Technol. 83, 82–90.
Lombardi, G., 1985. The Role of Cohesion in Cement Grouting of Rock. Commission Internationale, Lusanne, Switzerland.
Mitsoulis, E., 2007. Flows of viscoplastic materials: models and computations. Rheol. Rev. 135–178.
Mohajerani, S., Baghbanan, A., Wang, G., Forouhandeh, S.F., 2017. An efficient algorithm for simulating grout propagation in 2D discrete fracture networks. Int. J. Rock Mech. Min. Sci. 98, 67–77.
Nguyen, V.H., Rémond, S., Gallias, J.L., Bigas, J.P., Muller, P., 2006. Flow of Herschel-Bulkley fluids through the Marsh cone. J. Nonnewton. Fluid Mech. 139, 128–134.
Panaseti, P., Damianou, Y., Georgiou, G.C., Housiadas, K.D., 2018. Pressure-driven flow of a Herschel-Bulkley fluid with pressure-dependent rheological parameters. Phys. Fluids 30, 030701.
Pedrotti, M., Wong, C., El Mountassir, G., Lunn, R.J., 2017. An analytical model for the control of silica grout penetration in natural groundwater systems. Tunn. Undergr. Space Technol. 70, 105–113.
Rahman, M., Håkansson, U., Wiklund, J., 2015. In-line rheological measurements of cement grouts: effects of water/cement ratio and hydration. Tunnel. Undergr. Space Technol. 45, 34–42 ISSN 0886-7798.
Roustaei, A., Frigaard, I.A., 2013. The occurrence of fouling layers in the flow of a yield stress fluid along a wavy-walled channel. J. Non-Newtonian Fluid Mech. 198, 109–124 ISSN 0377-0257.
Saramito, P., Wachs, A., 2017. Progress in numerical simulation of yield stress fluid flows. Rheol. Acta 56 (3), 211–230.
Shamu, T.J., Håkansson, U., 2019. Rheology of cement grouts: On the critical shear rate and no-slip regime in the Couette geometry. Cem. Concr. Res. https://doi.org/10.1016/j.cemconres.2019.05.014. ISSN 0008-8846.
Stille, H., 2015. Rock Grouting: Theories and Applications. Vulkan Förlag.
Subramaniam, K.V., Wang, X., 2010. An investigation of microstructure evolution in cement paste through setting using ultrasonic and rheological measurements. Cem. Concr. Res. 40 (1), 33–44.
Sui, Wanghua, Liu, Jinyuan, Wei, Hu., Qi, Jianfeng, Zhan, Kaiyu, 2015. Experimental investigation on sealing efficiency of chemical grouting in rock fracture with flowing water. Tunn. Undergr. Space Technol. 50, 239–249.
U.S. Army Corps of Engineers, 2014. Drilling in Earth Embankment Dams and Levees. USA, U.S, Army Corps of Engineers, Washington, DC.
Wallner, M., 1976. Propagation of Sedimentation Stable Cement Pastes in Jointed Rock. Rock Mechanics and Waterways Construction. University of Aachen, BRD.
Wang, J.S.Y., Narasimhan, T.N., Scholz, C.H., 1988. Aperture correlation of a fractal fracture. J. Geophys. Res. 93 (B3), 2216–2224. https://doi.org/10.1029/JB093iB03p02216.
Warner, J., 2004. Practical Handbook of Grouting: Soil, Rock, and Structures. John Wiley & Sons, Hoboken, NJ, USA.
Xiao, Fei, Zhao, Zhiye, Chen, Huimei, 2017. A simplified model for predicting grout flow in fracture channels. Tunn. Undergr. Space Technol. 70, 11–18.
Xu, Zhipeng, Liu, Changwu, Zhou, Xingwang, Gao, Gangrong, Feng, Xuhai, 2019. Full-scale physical modelling of fissure grouting in deep underground rocks. Tunn. Undergr. Space Technol. 89, 249–261.
Zhao, Z., Li, B., Jiang, Y., 2014. Effects of fracture surface roughness on macroscopic fluid flow and solute transport in fracture networks. Rock Mech. Rock Eng. 47, 2279–2286.
Zhao, Z., Rutqvist, J., Leung, C., Hokr, M., Liu, Q., Neretnieks, I., Hoch, A., Havlíček, J., Wang, Y., Wang, Z., Wu, Y., Zimmerman, R., 2013. Impact of stress on solute transport in a fracture network: a comparison study. J. Rock Mech. Geotech. Eng. 5, 110–123.
Zhang, Qing-song, Zhang, Lian-zhen, Liu, Ren-tai, Li, Shu-cai, Zhang, Qian-qing, 2017. Grouting mechanism of quick setting slurry in rock fissure with consideration of viscosity variation with space. Tunn. Undergr. Space Technol. 70, 262–273.
Zou, L., Håkansson, U., Cvetkovic, V., 2019. Cement grout propagation in two-dimensional fracture networks: Impact of structure and hydraulic variability. Int. J. Rock Mech. Min. Sci. 115, 1–10.
Zou, L., Håkansson, U., Cvetkovic, V., 2018. Two-phase cement grout propagation in homogeneous water-saturated rock fractures. Int. J. Rock Mech. Min. Sci. 106, 243–249.
Zou, L., Jing, L., Cvetkovic, V., 2015. Roughness decomposition and nonlinear fluid flow in a single rock fracture. Int. J. Rock Mech. Min. Sci. 75, 102–118.
Zou, L., Jing, L., Cvetkovic, V., 2017a. Modeling of solute mixing at 3D rough-walled fracture intersections. Adv. Water Resour. 107, 1–9.
Zou, L., Jing, L., Cvetkovic, V., 2017b. Shear enhanced nonlinear flow in rough-walled rock fractures. Int. J. Rock Mech. Min. Sci. 97, 33–45.